ACS APPLIED MATERIALS & INTERFACES

Research Article

www.acsami.org

Effect of Size-Dependent Photodestructive Efficacy by Gold Nanomaterials with Multiphoton Laser

Wen-Tsan Chang,[†,Δ] Shean-Jen Chen,[‡,§,∥,Δ] Chia-Yuan Chang,[‡,§,Δ] Yi-Hsien Liu,[§] Chang-Hsin Chen,[⊥] Chen-Han Yang,[#] Lawrence Chao-Shan Chou,[‡,▽] Jui-Cheng Chang,[▽,¶] Li-Chung Cheng,[§] Wen-Shuo Kuo,[*,†,‡,∥,○,▲] and Jiu-Yao Wang[*,†,○,◆,▲]

[†]Department of Biochemistry and Molecular Biology, National Cheng Kung University, Tainan 701, Taiwan

[‡]Center for Micro/Nano Science and Technology, National Cheng Kung University, Tainan 701, Taiwan

[§]Department of Engineering Science, National Cheng Kung University, Tainan 701, Taiwan

[∥]Advanced Optoelectronic Technology Center, National Cheng Kung University, Tainan 701, Taiwan

[⊥]Antagene, Inc., Santa Clara, California 95054, United States

[#]Institute of Polymer Science and Engineering, National Taiwan University, Taipei 106, Taiwan

[▽]Department of Chemical Engineering, National Cheng Kung University, Tainan 701, Taiwan

[¶]Instrument Center, National Cheng Kung University, Tainan 701, Taiwan

[○]Allergy & Clinical Immunology Research Center, National Cheng Kung University, Tainan 701, Taiwan

[◆]Department of Pediatrics, National Cheng Kung University, Tainan 701, Taiwan

Supporting Information

ABSTRACT: The photostability, photodestructive efficacy, two-photon excitation cross section, and two-photon fluorescence of gold nanoparticles conjugated with a hydrophilic photosensitizer, indocyanine green, via multiphoton laser exhibited an increased size effect in methicillin-resistant *Staphylococcus aureus* and A549 cancer cells that was dependent on the size of multifunctional gold nanomaterials, but the effect only occurred when nanomaterials within 100 nm in diameter were used. Besides, the enhanced effectiveness of photodestruction, photostability, and contrast probe indicated an additive effect in the therapeutic and imaging efficiency of multifunctional gold nanomaterials. Consequently, the preparation of the multifunctional gold nanomaterials and their use in biomedical applications via multiphoton laser is an alternative and potential therapeutic approach for killing bacteria and for ablating cancer cells.

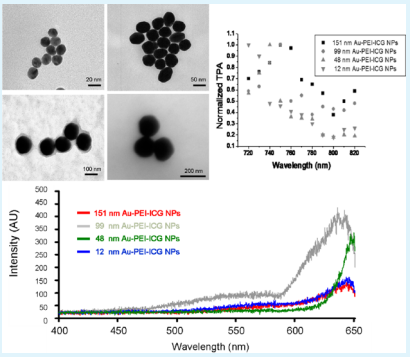

KEYWORDS: *photostability, photodestructive, two-photon action cross section, two-photon fluorescence, gold, methicillin-resistant Staphylococcus aureus, contrast probe*

INTRODUCTION

The continuous increase in the number of malignant species and multidrug-resistant bacterial strains and cancerous tumors is currently a critical problem, which is mainly caused by environmental variations occurring through different pathways, such as contamination, mutation, transformation, and metastasis, leading to a severe medical crisis. Hence, alternative approaches that eliminate the two malignant species must be developed. One of the currently major interests in new nanomaterials for nanomedicines is the use of near-infrared (NIR)-absorbing gold (Au)-based nanomaterials,[1,2] which have been extensively used in organisms because these materials are stable and biocompatible and can be used in the development of novel biological applications. These applications include effective signal enhancement, surface-enhanced Raman scattering, resonance light scattering, computed tomography scanning, and photothermal therapy (PTT).[3−6] The NIR region provides low scattering, energy absorption, and maximum irradiation penetration into deeper tissue.[2,6] Indocyanine green (ICG) is an anionic photosensitizer that absorbs in NIR window and is used in photodynamic therapy (PDT), which produces reactive oxygen species (ROS) to destroy and eliminate cancer cells and tissues via its photosensitizing property.[2,7] ICG has been approved by the U.S. Food and Drug Administration for medical diagnostic studies,[2] and it acts as a fluorescent contrast agent for enzymes and proteins and produces singlet oxygen, a type of ROS, that destroys cancer cells and tumors. Studies have reported that ICG is used to weld tissue with an NIR laser and provides a photothermal effect in clinical therapy.[8,9] Other studies have reported that Au nanostructures exert an effective

Received: May 21, 2015
Accepted: July 14, 2015
Published: July 14, 2015

DOI: 10.1021/acsami.5b04431
ACS Appl. Mater. Interfaces 2015, 7, 17318−17329

photothermal effect as well as varying in PTT efficiency depending on the sizes and shapes of Au-based nanomaterials.[2,10,11] However, no study has discussed the size-dependent photostability effect and photoparameters by using Au-based nanoparticle (NP)-conjugated ICG involving photodestruction and contrast probing through nonlinear multiphoton laser irradiation. Consequently, the interactions and photochemical reactions between excited photosensitizers and Au nanomaterials must be determined. This paper presents the use of ICG coupled with Au NPs of various sizes to simultaneously kill methicillin-resistant *Staphylococcus aureus* (MRSA) and destroy human lung carcinoma malignant cells (A549) through PDT and PTT administered using multiphoton laser irradiation. Compared with PDT or PTT treatment alone, the combined PDT–PTT ablation more efficiently destroyed the two malignant species. This work demonstrated the effect of size-dependent photostability, photodestruction, contrast agents, two-photon excitation cross section, and two-photon fluorescence when using Au nanomaterials.

MATERIALS AND EXPERIMENTS

Synthesis of Au–PEI–ICG NPs. Gold NPs were prepared by the procedure of the seedless growth method.[12] The surface charge of the 12 ± 0.83, 48 ± 1.22, 99 ± 2.19, and 151 ± 2.54 nm Au NPs was about −30.6, −37.3, −38.2, and −38.9 mV, respectively. Then, Au NPs were mixed with the positively charged polyethylenimine (PEI) polymer (Sigma-Aldrich Co., USA) to form Au–PEI NPs via electrostatic interaction.[2] The zeta potential of 12, 48, 99, and 151 nm Au–PEI NPs was 26.1, 28.3, 28.5, and 27.6 mV, respectively. Centrifuging the Au–PEI NPs solutions at 7500 rpm for 10 min was a necessary process to remove excess PEI. The pellets (Au–PEI NPs) were resuspended in ddH_2O and repeated several times. As-prepared all sizes of Au–PEI NPs/indocyanine green (ICG; TCI, Japan) by the particle number ratio of 1/70 000–1/150 000 were mixed for 5 h in aqueous solution. Via the electrostatic interaction, the 12, 48, 99, and 151 nm Au–PEI NPs were reacted with the negatively charged ICG to form Au–PEI–ICG NPs, respectively.[2] The zeta potential of 12, 48, 99, and 151 nm Au–PEI–ICG NPs was 15.1, 15.4, 15.5, and 15.0 mV, respectively. TEM image respectively depicts 12, 48, 99, and 151 nm Au–PEI–ICG NPs (Figure 1). Centrifuging (7500 rpm) the solutions for 10 min was a necessary process to remove excess ICG. The pellets (Au–PEI–ICG NPs) were resuspended in ddH_2O, and the centrifugation process was repeated several times. The concentration of Au NPs was calculated by the atomic absorption (AA) spectrometer (Solaar, UK).[2]

Characterization. Transmission electron microscopes (TEM) (JEOL 1400 and JEOL 2100, Japan) were used to characterize the morphology and energy dispersive X-ray (EDX) of the samples.[7] The ultraviolet–visible spectroscopy (UV–vis) absorption spectrometer (U-4100, Hitachi, Japan), Fourier transform infrared (FTIR) spectrometer (PerkinElmer RX1, USA), zeta potential spectrometer spectra (Manern Nano-ZS90, UK), and fluorescence spectrometer (FP-6600, JASCO)[2] were also used to determine the characters of samples.

Estimating the Average Amount of ICG per Au NPs. (1) Following previous studies,[2,7] we estimated by Lambert–Beer's law and measured with the AA spectrometer; the average amount of ICG for each size of Au NP was 22300 ICG molecules for each size of Au NP. (2) The intensity of a quantity of dissolved ICG in ddH_2O was recorded (Ex, 785 nm; Em, 815 nm). Via electrostatic interaction, Au–PEI–ICG NPs were mixed with the same quantify ICG in the dark for 5 h. Then, centrifuging (7500 rpm) the solutions for 10 min was a necessary process to remove excess ICG. The pellets (Au–PEI–ICG NPs) were resuspended in ddH_2O, and the centrifugation process was repeated several times. The difference in intensity between the collected supernatant and pure ICG was estimated. Following the AA spectrometer, the average amount of ICG was 22330 ICG molecules for each size of Au NP.

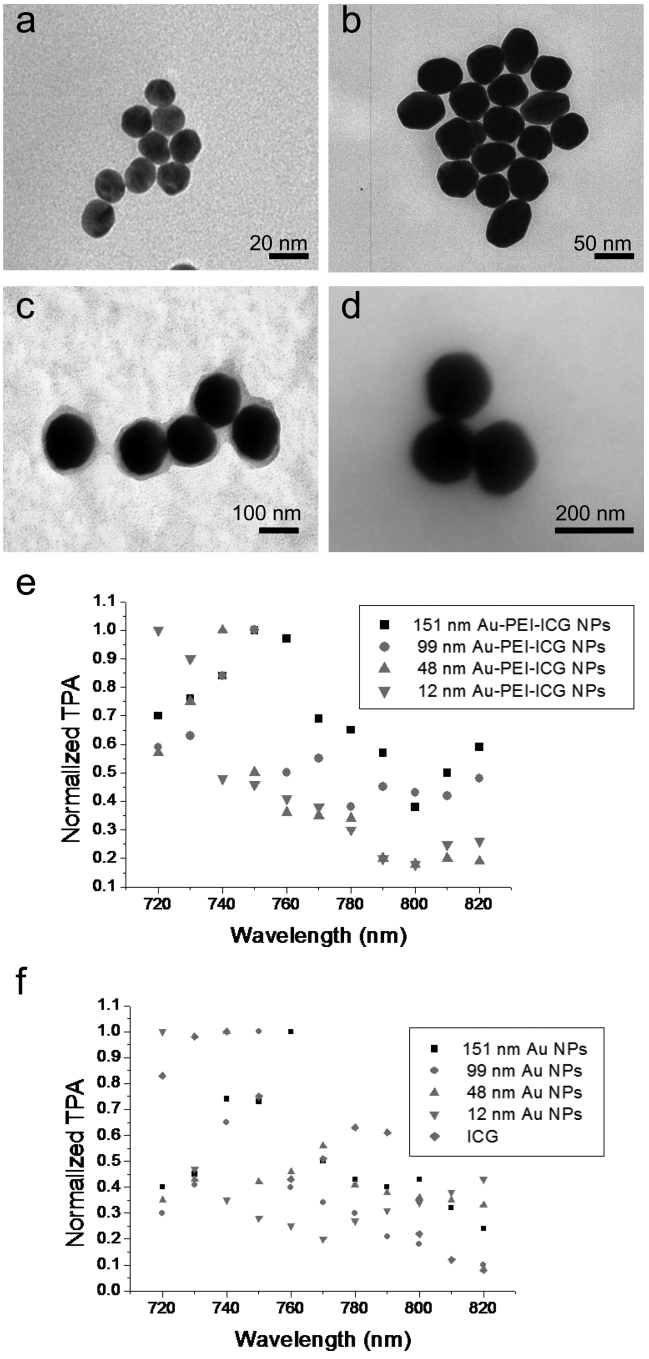

Figure 1. TEM micrographs of Au–PEI–ICG NPs with a diameter of (a) 12 ± 0.83, (b) 48 ± 1.22, (c) 99 ± 2.19, and (d) 151 ± 2.54 nm, respectively. Two-photon absorption (TPA) spectrum as a function of the excitation wavelength, (e) the relative TPA spectra of Au–PEI–ICG NPs, and (f) Au NPs and ICG. A femtosecond laser with a wavelength range of 720–820 nm was used to monitor TPA signals. Delivered dose, 1×10^{13} Au NPs (formula 1); 3.704×10^{-3} M of free ICG and ICG coated on the Au NPs.

After 4 days incubation of Au nanomaterials in aqueous solution,[2] desorbing ICG in aqueous solution for 12, 48, 99, and 151 nm Au nanomaterials, about 0.024, 0.031, 0.052, and 0.069%. In other words, PEI and ICG were successfully coated on the surfaces of the Au NPs in sequence. A proper amount of Au NPs was used in this study: 1×10^{13} Au NPs; 3.704×10^{-3} M of free ICG and ICG coated on the Au NPs.

DOI: 10.1021/acsami.5b04431
ACS Appl. Mater. Interfaces 2015, 7, 17318–17329

Bacterial Culture of MRSA.[1] This study was carried out using a strain of MRSA (ATCC 27659). Bacteria were grown in brain-heart infusion medium (DIFCO 0418; BD Biosciences, San Jose, CA). Bacteria were incubated at 37 °C.

Cell Culture of A549 Cells. The protocol to culture A549 cells followed previous studies.[1,7]

Antibodies Conjugation. For the improvement of specificity and therapeutic efficiency, ICG and all Au NPs and Au−PEI−ICG NPs were coated with the antiprotein A antibodies and antiepidermal growth factor receptor (EGFR) antibodies (Antagene, Inc., Santa Clara, CA), respectively.[2,7] ICG, and all Au NPs and Au−PEI−ICG NPs were respectively reacted with the antiprotein A antibody (1 mg mL^{-1}) and anti-EGFR antibody (1 mg mL^{-1}) for the ratio of $V_{antibody}/V_{material}$ = 1/1 at 4 °C for 30 min in the dark, respectively. Centrifuging (7500 rpm) the solutions for 15 min at 4 °C was a necessary process to remove excess antibodies. The pellets (Au−PEI−ICG NPs) were resuspended in 40 mM HEPES solution and the centrifugation process was repeated several times. The MRSA was respectively added to the ICG−$Ab_{protein\ A}$, Au NP−$Ab_{protein\ A}$, and Au−PEI−ICG NP−$Ab_{protein\ A}$ for 6 h of incubation in the dark at 37 °C, whereas the cell monolayer with A549 was respectively immersed with the ICG−Ab_{EGFR}, Au NP−Ab_{EGFR}, and Au−PEI−ICG NP−Ab_{EGFR} for 2 h, and then continued to go on the following experiment.[2,7]

Cytotoxicity Assay. *For MRSA.* MRSA (OD_{600} ~0.05) was respectively added to all the Au−PEI−ICG NPs $Ab_{protein\ A}$ (delivered dose: $1 \times 10^{11} \sim 1 \times 10^{13}$ Au NPs) and incubated in a 1.5 mL tube for 6 h of incubation in the dark at 37 °C. For the incubated bacteria, centrifuging (2000 rpm) the solutions for 10 min was a necessary process to remove excess Au nanommaterials or nonspecific binding. The pellets were resuspended in brain-heart infusion (nutrient medium), and the centrifugation process was repeated several times. The pellets were then diluted to a dilution factor of 10^{-4} to 10^{-9} and plated on the BD brain heart infusion agar plates. The plates were aerobically for 12−16 h of incubation in the dark at 37 °C. After incubation, the number of bacteria surviving by colony forming unit (CFU mL^{-1}) counting assay was determined.[2,7]

For A549 Cells. First, 5×10^3 cells per well in a 96-well culture plate were for overnight of incubation in the dark at 37 °C with 5% CO_2 in air. All of the Au−PEI−ICG NP−Ab_{EGFR} (delivered dose: 1×10^{11} to 1×10^{13} Au NPs) were respectively added to the incubated cells for overnight incubation in the dark at 37 °C. Medium was removed and replaced with the new culture medium, and the process was repeated three to five times to wash out the nonspecific binding. The cells were collected by trypsinization centriguged (1200 rpm) for 10 min to collect the pellets. Then, we followed previous studies[2,7] to conduct the MTT assay with an ELISA reader (Thermo Electron, Waltham, MA).

Evaluation of the Total Au Particle Number of Targeting and Internalization of Au Nanomaterials or Au Nanomaterials−Antibodies.[2,7,13] *For MRSA.* MRSA (OD_{600} ~ 0.05) was respectively added to all the Au−PEI−ICG NPs or Au−PEI−ICG NPs $Ab_{protein\ A}$ (dose: 1×10^{13} Au NPs) in a 1.5 mL tube for 12−16 h of incubation in the dark at 37 °C. For the incubated bacteria, centrifuging (2000 rpm) the solutions for 10 min was a necessary process to remove the nonspecific binding. The pellets were resuspended in brain-heart infusion (nutrient medium), which was repeated several times. Following the AA spectrometer (Solaar, UK) and formula 1, the amount of Au NPs was calculated. As a result, the total binding and uptaken Au particle number for each part of per Au−PEI−ICG NP-treated-bacterium or Au−PEI−ICG NP−$Ab_{protein\ A}$-treated-bacterium was calculated.

For A549 Cells. First, 5×10^3 cells per well in a 96-well culture plate were for overnight of incubation in the dark at 37 °C with 5% CO_2 in air. All of the Au−PEI−ICG NPs or Au−PEI−ICG NP−Ab_{EGFR} (dose: 1×10^{13} Au NPs) were respectively added to the incubated cells for overnight incubation in the dark at 37 °C. Medium was removed and replaced with the new culture medium, and the process was repeated three to five times to wash out the nonspecific binding. The cells were collected by trypsinization centriguged (1200 rpm) for 10 min to collect the pellets. Following the AA spectrometer (Solaar, UK) and formula 1, the amount of Au NPs (particle concentration of Au NPs) was calculated.

$$\text{amt of Au NPs} = \frac{\text{total no. of atoms}}{\text{Au atom nos. per Au NPs}} = \left(\frac{\frac{\text{concn of sample} \times \text{sample vol}}{\text{mol wt of Au}}}{\frac{\text{vol of Au nanosphere}}{\text{spherical vol of Au atom}}} \right) N_A \quad (1)$$

where the concentration of the sample is measured with an AA spectrometer, the molecular weight of Au is 197 g mol^{-1}, N_A is the Avogadro constant (6.02×10^{23}), the volume of Au nanosphere is (4/3) × 3.14 × (radius of Au NPs)^3, and the spherical volume of a Au atom is (4/3) × 3.14 × (atomic radius of Au)^3. As a result, the total binding and uptaken Au particle number for each part of per AAu−PEI−ICG NPs-treated sample or Au−PEI−ICG−Ab-treated sample was calculated:

$$\text{amt of targeting \& internalized Au} = \text{amt of Au NPs} \times \text{sample vol}$$

Femtosecond Laser Optical System for the Measurements of Photoluminescence, Two-Photon Absorption (TPA) and Two-Photon Photodestruction.[2,14−16] The homebuilt femtosecond Ti: sapphire laser optical system (repetition rate of 80 MHz) (Tsunami, Spectra-Physics, Santa Clara, CA) was used in this study.

TPA Measurement. A femtosecond laser with a wavelength range of 720−820 nm and was used to excite TPA signals. A time-average luminescence photon count (F) is proportional to the cross section (δ) of TPA and can be given as[17]

$$F \sim \frac{1}{2}\delta\eta_2\phi C\frac{g_p}{f\tau}\frac{8nP^2}{\pi\lambda} \quad (2)$$

where C is the concentration of the photoinitiator, η_2 is the quantum efficiency of photoluminescence, ϕ is the luminescence collection efficiency of the system, P is the average incident power, g_p is the dimensionless quantity for degree of the second-order temporal coherence, f is the pulse repetition rate, n is the refractive index of the measurement medium, λ is the excitation wavelength, and τ is the excitation pulse width by full-width at half-maximum. After the SF-10 prism pair compensation, the collection system, the pulse repetition rate, the concentration of the materials, and the excitation power can be maintained the same at different excitation wavelengths with their corresponding excitation pulse widths. On the basis of the measured excitation pulse width, the measured fluorescence photon count and the excitation wavelength, we derived the TPA as $\delta \times \eta_2$. Via the SPC module, the photomultiplier tubes were used to collect the photoluminescence photon counts. The TPA can be given as

$$\delta\eta_2 \propto \lambda\tau F \quad (3)$$

An in-lab constructed autocorrelator was used to monitor the pulse widths of the different wavelengths after the objective. With 2 m ms^{-1} speed of the galvanometer scanner, the excitation spectrum was measured to be 720−820 nm in wavelength with 3.0 mW excitation power. For the all size of Au−PEI−ICG NPs, Au NPs and ICG, Figure 1e,f shows the relative TPA spectrum as a function of excitation wavelength.

Photodestruction of MRSA and A549 Malignant Cells Shown by Fluorescence Images after Femtosecond Laser Irradiation. *Viability of MRSA after Photodestruction.* MRSA (OD_{600} ~ 0.05) were respectively added to all the Au−PEI−ICG NP−$Ab_{protein\ A}$, Au NP−$Ab_{protein\ A}$, and ICG−$Ab_{protein\ A}$ (delivered dose: 1×10^{13} Au NPs; 3.704×10^{-3} M of free ICG and ICG on the Au NPs) in a 1.5 mL tube to process the interaction of antibody−antigen for 6 h of incubation in the dark at 37 °C. For the incubated bacteria, centrifuging (2000 rpm) the solutions for 10 min was a necessary process to remove the nonspecific binding. The pellets were resuspended in brain-heart infusion (nutrient medium), and the centrifugation process was repeated several times. The pellets of incubated bacteria were diluted to OD_{600} ~ 0.05 and exposed to a

DOI: 10.1021/acsami.5b04431
ACS Appl. Mater. Interfaces 2015, 7, 17318−17329

femtosecond laser.[2,13] The irradiated-MRSA was stayed for 2.5 h of incubation in the dark at 37 °C to let the ICG proceed the PDT/PTT process (simultaneously, Au NPs proceeded PTT process). Following irradiation, the Au−PEI−ICG NP−$Ab_{protein\ A}$, Au NP−$Ab_{protein\ A}$, and ICG−$Ab_{protein\ A}$-treated MRSA were stained using a LIVE (SYTO 9, as indicated by green fluorescence)/DEAD (propidium iodide, as indicated by red fluorescence) kit (L7012, Invitrogen, Carlsbad, CA) following the instruction[18] and observed with a fluorescence microscopy (ECLIPSE TS100, Nikon, Japan). The number of bacteria surviving was determined by CFU method (CFU mL^{-1}). The Au−PEI−ICG NP−$Ab_{protein\ A}$, Au NP−$Ab_{protein\ A}$, and ICG−$Ab_{protein\ A}$-treated MRSA were diluted to a dilution factor of 10^{-4} to 10^{-9} and plated on the BD brain heart infusion (BHI) agar plates. The plated were incubated aerobically at 37 °C for 12−16 h in the dark. After incubation, the number of bacteria surviving (CFU mL^{-1}) was calculated.[1,2]

Viability of A549 Cells after Photodestruction. First, 5 ×10^3 A549 cells per well in a 96-well culture plate were incubated overnight in the dark at 37 °C with 5% CO_2 in air. All of the Au−PEI−ICG NPs or Au−PEI−ICG NP−Ab_{EGFR} (delivered dose: 1 × 10^{13} Au NPs; 3.704 × 10^{-3} M of free ICG and ICG on the Au NPs) were respectively added to the incubated cells to process the interaction of antibody−antigen for 2.5 h of incubation in the dark at 37 °C. Medium was removed and replaced with the new culture medium, and the process was repeated three to five times to wash out the nonspecific binding. Subsequently, the cells were stained with calcein AM (Invitrogen Corp., Carlsbad, CA) for 2.5 h of incubation in the dark at 37 °C [2] to let the ICG proceed the PDT/PTT process (simultaneously, Au NPs proceeded PTT process) following femtosceond laser exposure. Produced green fluorescence stood for the viable cells, and then observed by a fluorescence microscopy and analyzed images with ImageJ software. For MRSA and A549 cells, excited wavelength: 720 nm (for 12 nm Au NPs and Au nanomaterials), 740 nm (for 48 nm Au NPs and Au nanomaterials), 750 nm (for 99 nm Au NPs and Au nanomaterials) and 760 nm (for 151 nm Au NPs and Au nanomaterials) at a power of 5.0 mW for 40, 30, 20, and 50 s, respectively; 740 nm (for ICG) with 5.0 mW and 50 s irradiation; 720 nm (control experiment) with 20 mW exposure for 90 s; delivered flux, 13939 W mm^{-2} (for 720 nm), 13227 W mm^{-2} (for 740 nm), 12853 W mm^{-2} (for 750 nm), and 12531 W mm^{-2} (for 760 nm); total energy dose: 557 560 J (for 12 nm Au NPs and Au nanomaterials), 396810 J (for 48 nm Au NPs and Au nanomaterials), 257 060 J (for 99 nm Au NPs and Au nanomaterials), 626 550 J (for 151 nm Au NPs and Au nanomaterials), 661 350 J (for ICG), and 5 017 860 J (for control experiment) (n=6).

Detection of ROS. *Singlet Oxygen.*[1,2,7] ICG and all Au nanomaterials were irradiated with the femtosecond laser in the dark (excited wavelength: 720 nm for 12 nm Au NPs, 740 nm for 48 nm Au NPs, 750 nm for 99 nm Au NPs, and 760 nm for 151 nm Au NPs at a power of 5.0 mW for 40, 30, 20, and 50 s, respectively; 740 nm for ICG with 5.0 mW and 50 s irradiation) and then directly detect singlet oxygen (Ex/Em: 488/525 nm) by the treatment of 1 mM of Singlet Oxygen Sensor Green Reagent (Invitrogen Corp., Grand Island, NY), and the data were collected by a fluorescence spectrophotometer. Delivered dose: 1 × 10^{13} Au NPs; 3.704 × 10^{-3} M of free ICG and ICG on the Au NPs. Data are means ± SD (n = 6).

Superoxide Radical Anion.[18,19] The A549 cancer cells (5 × 10^3 cells per well in a 96-well culture plate) were seeded into ICG and all Au nanomaterials for overnight of incubation in the dark at 37 °C with 5% CO_2 in air. After they had been incubated, the mixture exposed to nonlinear laser in the dark. Excited wavelength: 720 nm (for 12 nm Au nanomaterial-treated cells), 740 nm (for 48 nm Au nanomaterials-treated-cells), 750 nm (for 99 nm Au nanomaterial-treated cells) and 760 nm (for 151 nm Au nanomaterials-treated-cells) at a power of 5.0 mW for 40, 30, 20, and 50 s, respectively, whereas 740 nm (for ICG-treated-cells) with 5.0 mW and 50 s irradiation, and then mixed with 1 mL 0.45 mM XTT (Fluka, USA) for 5 h of incubation in the dark. XTT would interact with superoxide radical anion and form the XTT-formazan showing strong absorption at 470 nm in wavelength. Measurement of absorption was recorded by UV−vis spectrometer. Delivered flux: 13 939 W mm^{-2} (for 720 nm), 13 227 W mm^{-2} (for 740 nm), 12 853 W mm^{-2} (for 750 nm) and 12531 W mm^{-2} (for 760 nm); total energy dose: 557 560 J (for 12 nm Au NPs and Au nanomaterials), 396 810 J (for 48 nm Au NPs and Au nanomaterials), 257 060 J (for 99 nm Au NPs and Au nanomaterials), 626 550 J (for 151 nm Au NPs and Au nanomaterials), 661 350 J (for ICG) and 5 017 860 J (for control experiment). Delivered dose: 1 × 10^{13} Au NPs; 3.704 × 10^{-3} M of free ICG and ICG on the Au NPs. Data are means ± SD (n = 6).

Cytotoxicity of A549 Cells for Long-Term.[2,7] Cells (5 × 10^3 cells per well in a 96-well culture plate) were seeded into ICG and all Au nanomaterials for overnight incubation in the dark at 37 °C with 5% CO_2 in air. ICG−Ab_{EGFR} and 151 nm Au−PEI−ICG NP−Ab_{EGFR} were irradiated with a femtosecond laser (740 nm for ICG−Ab_{EGFR}, and 760 nm for 151 nm Au−PEI−ICG NP−Ab_{EGFR}) at 5.0 mW for 50 s first to test the photostability of ICG and Au nanomaterials and then added to the confluent cells in a 96-well culture plate and continued for an additional 2 h, 1 day, and 4 days of incubation in the dark at 37 °C with 5% CO_2 in air, respectively. Medium was removed and replaced with the new culture medium and repeat for 3 to 5 times to wash out the nonspecific binding. The cells were collected by trypsinization and centrifuged (1200 rpm) for 10 min to collect the pellets. Then, we followed previous studies[2,7] to conduct the MTT assay with an ELISA reader (Thermo Electron, Waltham, MA). Delivered dose: 1 × 10^{13} Au NPs; 3.704 × 10^{-3} M of free ICG and ICG on the Au NPs.

Measurement of Two-Photon Excitation Action Cross Section. The two-photon excitation action cross section was measured the fluorescence signal via femtosecond laser optical system mentioned above. The back aperture of the 20× objective lens (NA 0.256) was overfilled by expansion of the laser beams. For the multiphoton excitation, the diffraction-limited illumination of the sample was approximately achieved and analyzed. Under two-photon excitation and for the thick sample limit, the relation between time-averaged fluorescence photon flux $\langle F^{(n)}(t)\rangle$ and the incident power $P(t)$ can be obtained. The formula can be given as[20]

$$\langle F^{(n)}(t)\rangle = \frac{1}{n}\frac{g_p^{(n)}}{(f\tau)^{n-1}}\phi\eta\sigma_n C n_0 \frac{a_n(\mathrm{NA})^{2n-4}\langle P(t)\rangle^n}{8\pi^{3-n}\lambda^{2n-3}} \quad (4)$$

where C is the concentration of the fluorophore, n is the number of photons absorbed (n = 2 for the two-photon excitation), ϕ is the system collection efficiency, τ is the laser pulse width, f is the laser repetition rate, η is the fluorescence quantum efficiency, and λ is the excitation wavelength in vacuum, σ_n is the n-photon absorption cross section, and a_2 = 64 for two-photon excitation. $g_p^{(n)}$ is the n^{th}-order temporal coherence of the excitation source. Due to the limitation of resources we currently have, $\langle F^{(n)}(t)\rangle$ is temporarily not able to be calculated, and the values could be replaced by the integrated two-photon fluorescence intensity with the symbol of "counts". As a result, the equation for action cross section ($\eta\sigma_2$) is turned into[21]

$$\eta\sigma_2 = \frac{\mathrm{counts}}{\frac{1}{2}\frac{g_p^{(2)}}{f_\tau} n_0\phi C\frac{8\langle P(t)\rangle^2}{\pi\lambda}} \quad (5)$$

If it was with the same second-order temporal coherence of the excitation source, the laser pulse width, laser repetition rate, incident power, system collection efficiency, wavelength and working concentration, the action cross section of two-photon excitation ($\eta\sigma_2$) for a fluorophore as the reference compound is determined relative to the known action cross section, then formula 5 is simplified as

$$(\eta\sigma_2)_2 = \frac{\mathrm{counts}_2}{\mathrm{counts}_1}(\eta\sigma_2)_1 \quad (6)$$

where sample 1 is the reference compound, and sample 2 is the fluorophore.

For careful concern, the known action cross section of two-photon excitation for fluorescein and Rhodamine B (Sigma-Aldrich Co., St. Loius, MO) was first used as the standard reference and fluorophore to

DOI: 10.1021/acsami.5b04431
ACS Appl. Mater. Interfaces 2015, 7, 17318−17329

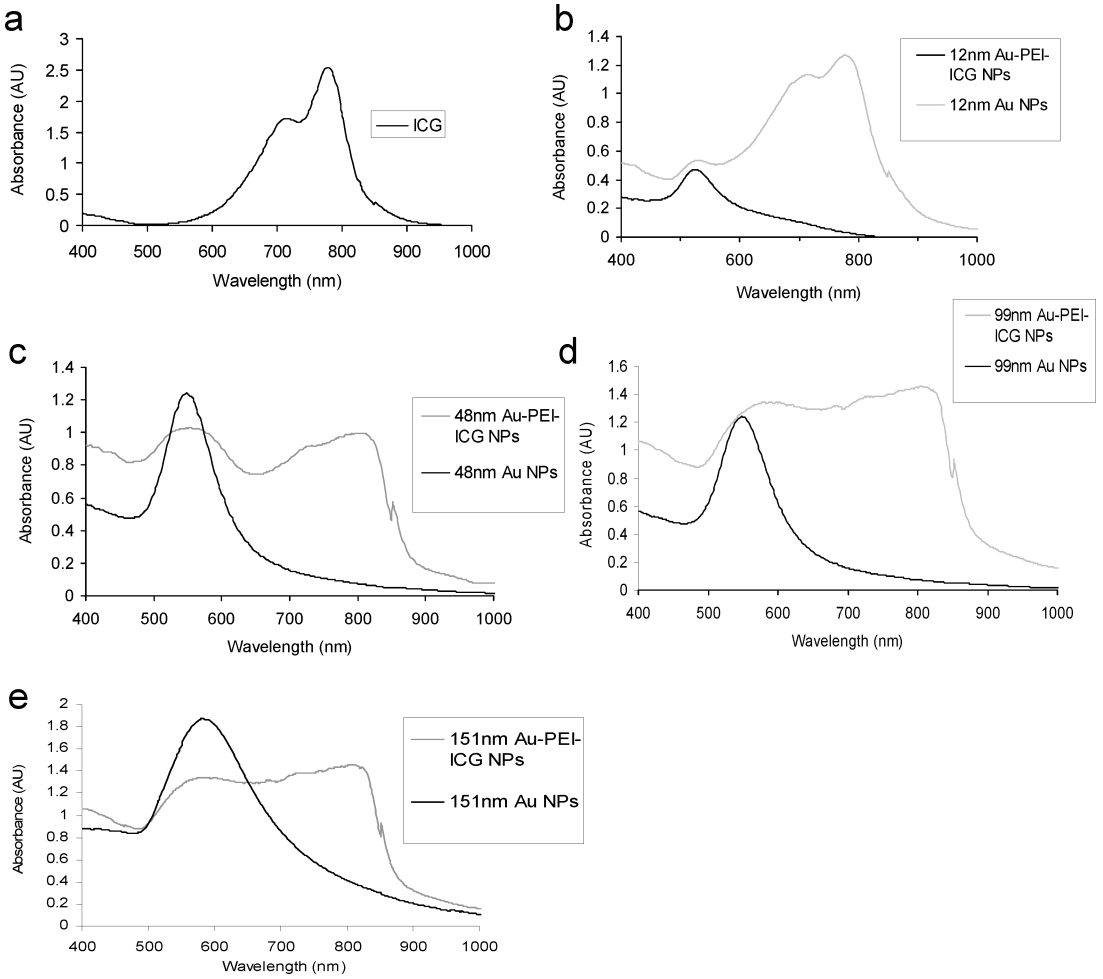

Figure 2. UV−vis spectra of (a) ICG, (b) 12 nm Au−PEI−ICG NPs (plasmon resonance of 12 nm Au NPs, ca. 520 nm), (c) 48 nm Au−PEI−ICG NPs (plasmon resonance of 48 nm Au NPs, ca. 547 nm), (d) 99 nm Au−PEI−ICG NPs (plasmon resonance of 99 nm Au NPs, ca. 564 nm), and (e) 151 nm Au−PEI−ICG NPs (plasmon resonance of 151 nm Au NPs, ca. 580 nm). Delivered dose: 1×10^{10} Au NPs mL^{-1}.

calculate each other's action cross section and vice versa. At 750 nm in wavelength of femtosecond laser exposure, the action cross section of two-photon excitation for fluorescein and Rhodamine B is 33.6 and 55.0 GM (1 GM = 10^{-50} cm^4 s $photon^{-1}$),[20−22] respectively. The integrated two-photon fluorescence (TPF) intensity for Counts was based on the spectra (Supporting Information, Figure S1). By measuring the dependence of the emission intensity on the excitation power range of 20−80 mW, the results were shown in Figure S2 (Supporting Information); moreover, TPF of fluorescein and Rhodamine B was needed to be verified.[23] In each figure, the slopes of the lines were to determine the fluorescence from two-photon excitation. Based on formula 6,[21] the two-photon excitation action cross section of fluorescein and Rhodamine B could be calculated as 35.1 and 56.5 GM (Supporting Information, Table S1). Compared to the data in the previous studies, there is only 5% in error that is the acceptable deviation. In other words, the action cross section of two-photon excitation for sample was available via formulas 5 and 6. We followed this method and selected Rhodamine B as a standard reference,[20−22] and thus, the action cross sections of two-photon excitation for 12, 48, 99, and 151 nm Au−PEI−ICG NPs can be obtained, respectively.

Measurement of TPF Spectrum.[2,14,15] All sizes of Au nanomaterials were exposed to femtosecond laser, respectively. Excited wavelength: 720 nm for 12 nm Au NPs and Au−PEI−ICG NPs, 740 nm for 48 nm Au NPs and Au−PEI−ICG NPs, 750 nm for 99 nm Au NPs and Au−PEI−ICG NPs, 760 nm for 151 nm Au NPs and Au−PEI−ICG NPs at a power of 5.0 mW. Scanning area 200 × 200 μm^2, frequency: 10 kHz, a duration of 1.638 s exposure time/scan = 100 μs per pixel per scan, 128 × 128 pixels/scan, pixel area = 1562.5 × 1562.5 nm^2. For 720, 740, 750, and 760 nm excitation: the total irradiation time t = 3.670 ms × number of scans, t = 3.877 ms × number of scans and obtain the data, t = 3.98 ms × number of scans and obtain the data, and t = 4.078 ms × number of scans and obtain the data, respectively. A 40× oil-immersion objective (NA 1.3) was used to collect the signals, and the detection range of spectrum photometer was 400−650 nm in wavelength.

Statistical Analysis. The statistical significance of the viable bacteria or cell (%) with different treatment concentrations were by the analysis of variance. In all cases, the p-value <0.05 was considered statistically significant. The methods of related and further analysis were followed the previous study.[24]

RESULTS AND DISCUSSION

Au NPs exposing carboxyl group were synthesized,[12] and ICG was conjugated on their surfaces. Subsequently, positively charged PEI and negatively charged ICG were coated in sequence through electrostatic interaction on the surface of the NPs. TEM images show 12, 48, 99, and 151 nm Au−PEI−ICG NPs (Figure 1a−d). Because of the carboxyl group, the surface charge of the 12 nm Au NPs was approximately −30.6 mV, whereas that of the 48, 99, and 151 nm Au NPs was −37.3, −38.2, and −38.9 mV, respectively. PEI and ICG were then absorbed in sequence by Au NPs of all sizes by electrostatic interactions, and therefore the surface charge of 12, 48, 99, and

DOI: 10.1021/acsami.5b04431
ACS Appl. Mater. Interfaces 2015, 7, 17318−17329

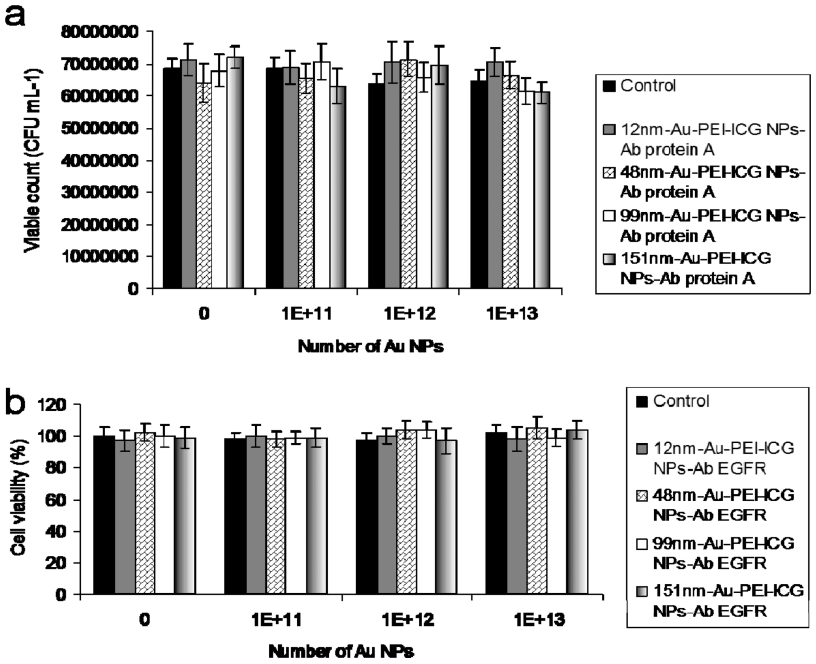

Figure 3. Viability of (a) all sizes of Au−PEI−ICG NP-antibodie-treated MRSA and (b) A549 cells was estimated.[2] Delivered dose: $1 \times 10^{11} \sim 1 \times 10^{13}$ Au NPs. Data are means ± SD (n = 6).

Table 1. Evaluation of the Au Particle Number Per Bacterium or Cell of Specific Targeting or Internalization of Au−PEI−ICG NP−$Ab_{protein\ A}$ for MRSA and Au−PEI−ICG NP−Ab_{EGFR} for A549 Cells, Respectively

	12 nm Au−PEI−ICG NPs−antibodies	48 nm Au−PEI−ICG NPs−antibodies	99 nm Au−PEI−ICG NPs−antibodies	151 nm Au−PEI−ICG NPs−antibodies
MRSA	150	92	60	38
A549 cells	358	225	75	51

151 nm Au−PEI−ICG NPs was approximately −15.1, −15.4, −15.5, and −15.0 mV, respectively. The spectra for ICG consisted of two main peaks at approximately 708 and 780 nm, which meant oligomeric and monomeric forms, respectively, by the confirmation of UV−vis[7] (Figure 2a). The Au NPs with various sizes exhibited plasmon resonances (approximately 520−580 nm), and the plasmons gradually had a red shift absorption with the enlargement of the NPs (Figure 2b−e). When PEI and ICG were conjugated in sequence on the Au NPs, two additional bands appeared around 708 and 780 nm. Surface modification of metallic NPs with organic molecules results in highly ordered structures and superstructures.[25−27] The electron density of the metallic NPs was changed by chemical interactions, thereby directly affecting the absorption of the conjugation on the surface of organic molecules and the absorption band of the surface plasmon.[26,28] Successful conjugation of the Au−PEI−ICG NPs was proved by the information from UV−vis spectra. In addition, according to the absorbance difference of ICG at 780 nm before and after ICG was conjugated with the Au NPs, approximately 22 300 ICG molecules conjugated per Au-PEI NP of each size, according to the Lambert−Beer law.[1,2,7] The other quantification assay was conducted by fluorescence spectrometer. An average of about 22 330 ICG molecules for each Au-PEI NP was determined. To manifest the effect of size-dependence photodestructive efficacy by Au nanomaterials, we painstakingly controlled the average of ICG per Au NPs to be almost the same quantity. In this way, we can expound the results clearly. After incubating Au nanomaterials in an aqueous solution for 4 days, 12 nm Au nanomaterials desorbed approximately 0.024% of ICG in the aqueous solution, whereas 48, 99, and 151 nm Au nanomaterials desorbed approximately 0.031, 0.052, and 0.069%, respectively, of ICG in the solution. Furthermore, we determined the size stability of Au nanomaterials of all sizes, and we found no size variation, indicating no further desorption of conjugated ICG after 4 days of incubation in the aqueous solution (Supporting Information, Figure S3). The FTIR spectra were utilized to analyze exposed functional groups of the Au nanomaterials (Supporting Information, Figure S4). These results show that PEI and ICG were well coated on the surfaces of Au NPs in sequence.

In this study, Gram-positive MRSA and A549 cancer cells were selected as experimental templates. Great interest exists in developing alternative treatments to eliminate bacterial and malignant cells, and Au-based multifunctional nanomaterials show the ability and efficacy to destroy these two cell types. Before proceeding with photodestruction, the biocompatibility of the Au nanomaterial-treated MRSA and A549 was examined. Protein A is a surface protein found in the cell wall of MRSA, and EGFR overexpresses on the surface of A549 cells.[2] The antiprotein A ($Ab_{protein\ A}$) and anti-EGFR antibodies (Ab_{EGFR}) were respectively coated with ICG and Au−PEI−ICG NPs to efficiently target the multiphoton photochemical destruction; subsequently, the Au−PEI−ICG NP−$Ab_{protein\ A}$ and Au−PEI−ICG NP−Ab_{EGFR} were treated with MRSA and A549 cells, respectively. Experiments for MRSA and A549 cell viability were performed by incubating MRSA and A549 cells overnight with Au−PEI−ICG NP−$Ab_{protein\ A}$ and Au−PEI−ICG NP−Ab_{EGFR}, respectively, in the dark, as well as all of the following photodestruction experiments involving ICG.[2] The viabilities of MRSA and A549 cells were almost 100%, indicating high biocompatibility (Figure 3 and Supporting Information, Figure

DOI: 10.1021/acsami.5b04431
ACS Appl. Mater. Interfaces 2015, 7, 17318−17329

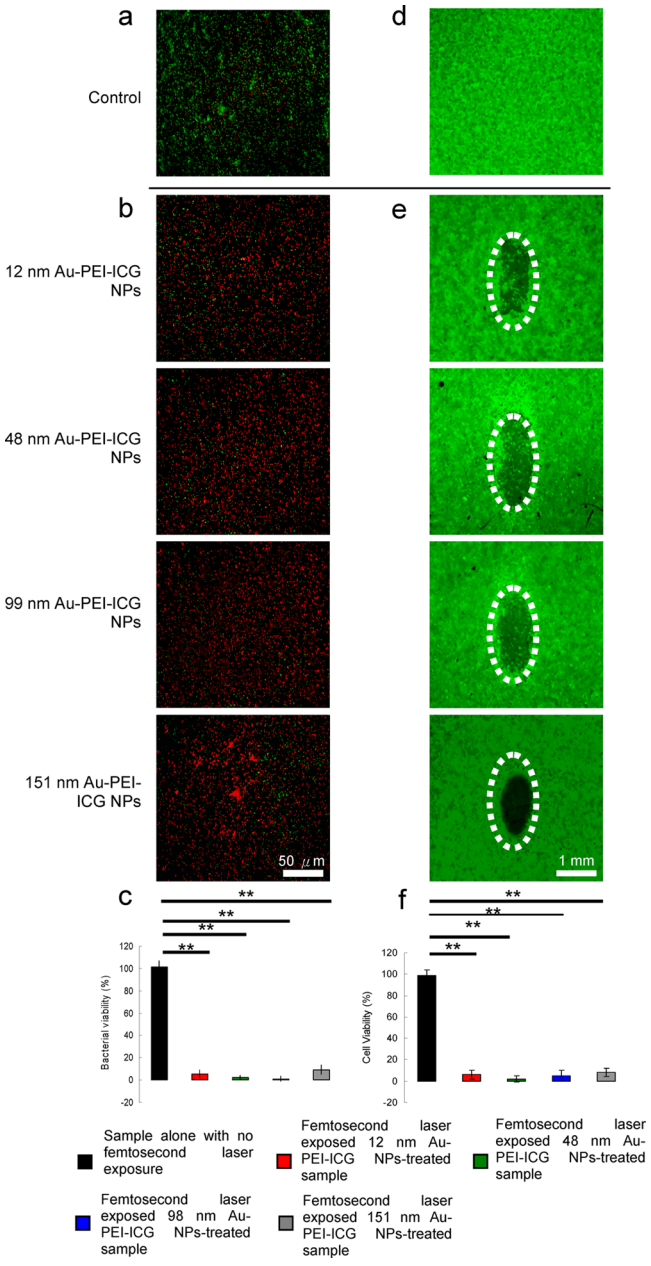

Figure 4. (a–c) Photodestruction of MRSA shown by fluorescence. (a and b) Images and viabilities of MRSA after they were treated with Au–PEI–ICG NP–$Ab_{protein\ A}$ and then exposed to the femtosecond laser. MRSA were stained using a LIVE/DEAD kit to obtain the fluorescent images, and (c) quantification for viability was estimated. (d and e) Different sizes of Au–PEI–ICG NP–Ab_{EGFR}-treated A549 cells were exposed by the femtosecond laser[2] with the indication of the laser beam spots in dotted circles. After exposure to laser, the live cells exhibited green fluorescence that was emitted from the calcein AM staining. (f) Estimation of cell viability of Au–PEI–ICG NP–Ab_{EGFR}-treated A549 cells. Data are means ± SD (n = 6). **p value obtained by Student's t test.

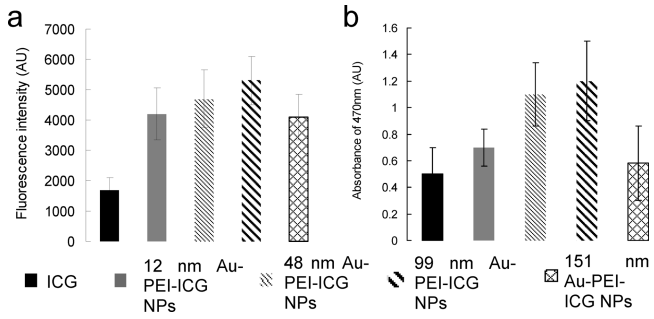

Figure 5. Measurements of (a) singlet oxygen and (b) superoxide radical anion were done, respectively. ICG and all Au nanomaterials were exposed to femtosecond laser in the dark. Delivered dose: 1×10^{13} Au NPs; 3.704×10^{-3} M of free ICG and ICG coated on the Au NPs. Data are means ± SD (n = 6).

S5). In all the experiments of this work, for each size of the Au NPs, we chose an appropriate number of NPs (1×10^{13}), which were then conjugated with similar quantities of ICG at 3.704×10^{-4} M. We also calculated the Au particle number per bacterial or cellular targeting and internalization for each part through the AA spectrometry analysis (Table 1). No antibody coated Au–PEI–ICG NPs were used to conduct the targeting or internalization experiment (Supporting Information, Table S2). The internalized Au particle number dramatically decreased. The results showed that not only the antibodies were well coated on the Au–PEI–ICG NPs surfaces but also as the particle size increased, the quantity of particles binding onto or absorbed by bacteria and cells decreased.

ICG and Au nanomaterials exhibit absorption in the NIR region and exhibit photothermal properties. By themselves, biocompatible Au nanomaterials might show photodestructive ability toward cancer cells exposed to nonlinear multiphoton laser irradiation. Conversely, because of the noninvasive property of suborganismic features with <1 mm deep penetration into tissue,[2] using nonlinear excitation could have the added advantage of shortening the exposure time, maintaining a low average laser power, and allowing the excitation window to be extended to the IR region, which makes the process more visible when it is applied for organisms that are not transparent to visible wavelengths. The measurement of the TPA spectrum was conducted before performing the photodestruction experiments.[7,14,15] We discovered that the most efficacious excitation wavelengths for the relative TPA maximum ratio of 12, 48, 99, and 151 nm Au–PEI–ICG NPs were approximately 720, 740, 750, and 760 nm, respectively (Figure 1e); the maximum ratios of the relative TPA[29] of the 12, 48, 99, and 151 nm Au NPs were asspproximately 720, 740, 750, and 760 nm, respectively, and was 740 nm for ICG alone (Figure 1f). Due to good absorption in the near-infrared window, the biocompatible Au nanomaterials possessed the ability to detect deeper tissue and simultaneously were able to apply in biomedical field via nonlinear laser throughout this work. MRSA treated with 12 nm Au–PEI–ICG NP–$Ab_{protein\ A}$ after multiphoton laser exposure were stained and imaged.[14] The laser-exposed bacteria alone exhibited almost no damage, as shown by the predominance of green fluorescence, indicating live bacteria (Figure 4a). However, the number of dead bacteria was discernible to a certain extent in both treatments of Au nanomaterials and laser irradiation, as indicated by the predominance of red fluorescence (Figure 4b). To further elucidate the efficacy of photothermolytic antimicrobial ability shown in Figure 4a,b, bacterial viability were quantified.[1,2] After exposure, viability was significantly lower in MRSA treated with 12, 48, 99, and 151 nm Au–PEI–ICG NPs $Ab_{protein\ A}$ than in those without exposure (7.5 vs 101%, 3.3 vs 101%, 2.1 vs 101%, and 12.4 vs 101%; p = 0.000094, p = 0.00008, p = 0.000072, and p = 0.000113, compared with bacteria treated with exposure alone, respectively (Figure 4c). Results of the CFU

DOI: 10.1021/acsami.5b04431
ACS Appl. Mater. Interfaces 2015, 7, 17318–17329

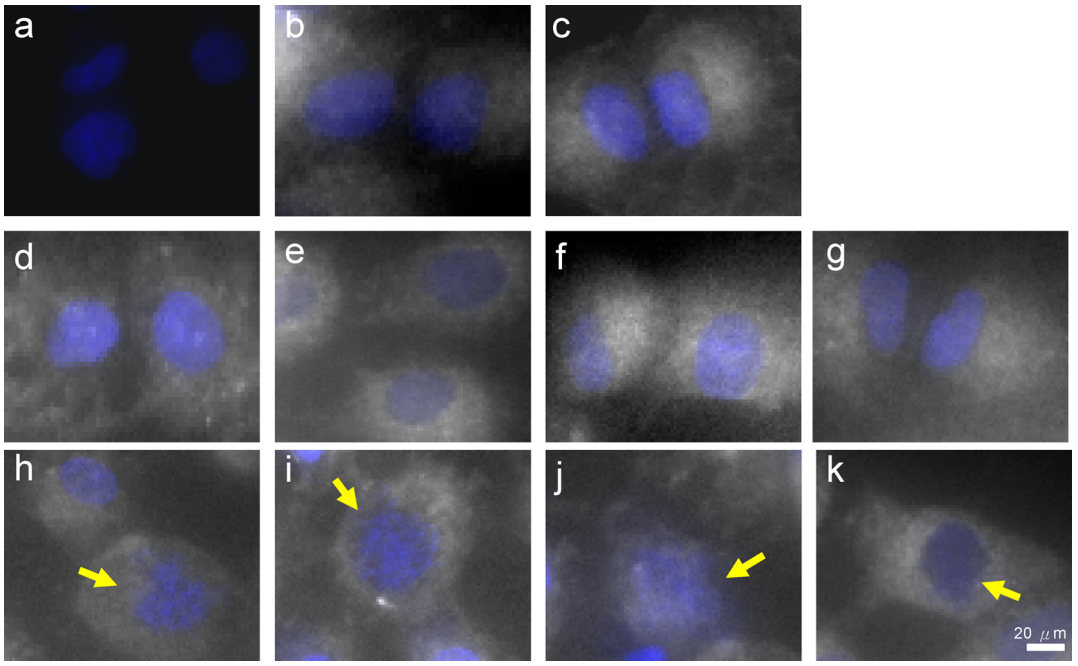

Figure 6. Images of A549 cancer cells (a) without ICG−Ab_{EGFR} treatment or femtosecond laser exposure, (b) with ICG−Ab_{EGFR} treatment but without laser exposure, (c) with ICG−Ab_{EGFR} treatment and with laser exposure, (d−g) with 12, 48, 99, and 151 nm Au−PEI−ICG NP−Ab_{EGFR} treatment, respectively, but without laser exposure, and (h−k) with 12, 48, 99, and 151 nm Au−PEI−ICG NP−Ab_{EGFR} treatment, respectively, and with laser exposure. Cells were then observed using laser confocal microscopy. The nuclei were stained with DAPI (blue). Excited wavelength: 720 nm (12 nm Au NP- and 12 nm Au nanomaterial-treated cells), 740 nm (48 nm Au NP- and 48 nm Au nanomaterial-treated cells), 750 nm (99 nm Au NP- and 99 nm Au nanomaterial-treated cells) and 760 nm (151 nm Au NP- and Au nanomaterial-treated cells) at a power of 5.0 mW for 40, 30, 20, and 50 s, respectively, whereas 740 nm (for ICG-treated cells) with 5.0 mW and 50 s irradiation. Delivered dose: 1×10^{13} Au NPs; 3.704×10^{-3} M of free ICG and ICG coated on the Au NPs.

counting method were similar to those of the viability quantified using a LIVE/DEAD kit (Supporting Information Figure S6).[1,2] Despite a longer multiphoton laser exposure, the viability of 151 nm Au−PEI−ICG NP−$Ab_{protein\ A}$-treated MRSA was higher than that of others. Concurrently, Figure S7a−c (Supporting Information) shows that the viabilities of ICG−$Ab_{protein\ A}$-treated, 12 nm Au NP−$Ab_{protein\ A}$-treated, 48 nm Au NP−$Ab_{protein\ A}$-treated, 99 nm Au NP−$Ab_{protein\ A}$-treated, and 151 nm Au NP−$Ab_{protein\ A}$-treated MRSA dropped to 79, 63, 66, 60, and 64%, respectively. In other words, the Au−PEI−ICG NPs exerted an additive effect of photodestruction compared with ICG alone and Au NPs, resulting in at least a 47% increase in therapeutic efficacy.[1,2,7] By contrast, in A549 cells, a substantial loss in viability, marked by an insufficient green fluorescence emitted from the calcein AM-stained cells,[7] occurred after treatment with Au−PEI−ICG NP−Ab_{EGFR} and Au NP−Ab_{EGFR} of various sizes and exposure times (Figure 4d,e); however, the A549 cells treated with irradiation alone showed no loss of viability. Cell viability (%) was determined by dividing the integrated green fluorescence light intensity by the fluorescence intensity of the control cells with the indication of the laser beam spots in dotted circles[7] (Figure 4f). The viability of the 12, 48, and 99 nm Au−PEI−ICG NP−Ab_{EGFR}-treated A549 cells decreased to <10% (p = 0.000083, 0.000079, and 0.000056 for the viability of the controls compared with each size), respectively. However, even after a longer laser exposure, the viability of 151 nm Au−PEI−ICG NP−Ab_{EGFR}-treated A549 cells only fell to 15% (p = 0.000124), but the viabilities of ICG−Ab_{EGFR} and Au NP−Ab_{EGFR}-treated cells still exhibited 80% (Supporting Information, Figure S7d−f). Consequently, an additive effect with at least 65% enhancement was confirmed in the therapeutic efficacy of Au−PEI−ICG NP−Ab_{EGFR}-treated A549 cells. In addition, the quantity of the singlet oxygen generated by ROS from the Au−PEI−ICG NPs was higher than that generated by ICG alone, but a size-dependent and additive effect was observed (Figure 5a). However, singlet oxygen and hydroxyl radicals can be derived from superoxide anions.[30] The results of the generated superoxide anion were similar to those of the generated singlet oxygen (Figure 5b). No matter the laser-irradiated bacteria, cancer cells, or generated ROS, the 99 nm Au NPs, only exposed for 20 s, were able to develop the best efficacy; but the 151 nm Au NPs had the worst ability to achieve similar results by the longest exposure time. The increase of ROS generated by Au nanomaterials might have been due to increased triplet yield, enhanced intersystem crossing of the ICG or the Au materials, resulting in photostability of the ICG on the Au NPs and improve the photodestructive efficacy.[1,31,32] In summary, in the Au NPs with a diameter within 100 nm, the apparent photodestructive effect was exhibited and occurred as the size of the nanomaterials increased, but in the NPs with a diameter over 100 nm, a recessive phenomenon was exhibited; moreover, ICG clearly exhibited photodestructive efficacy after conjugation with the Au NPs.

Because Au−PEI−ICG NPs are a contrast probe of ICG, the potential of multimodal agents with photodestruction and optical imaging increases with the integration of the characteristics of the NPs.[1,7] The images of ICG−Ab_{EGFR}-treated A549 cells without and with femtosecond laser exposure are shown in Figure 6b,c. Au particles were absorbed into cells and showed considerable NIR fluorescence emitted from ICG (one-photon

DOI: 10.1021/acsami.5b04431
ACS Appl. Mater. Interfaces 2015, 7, 17318−17329

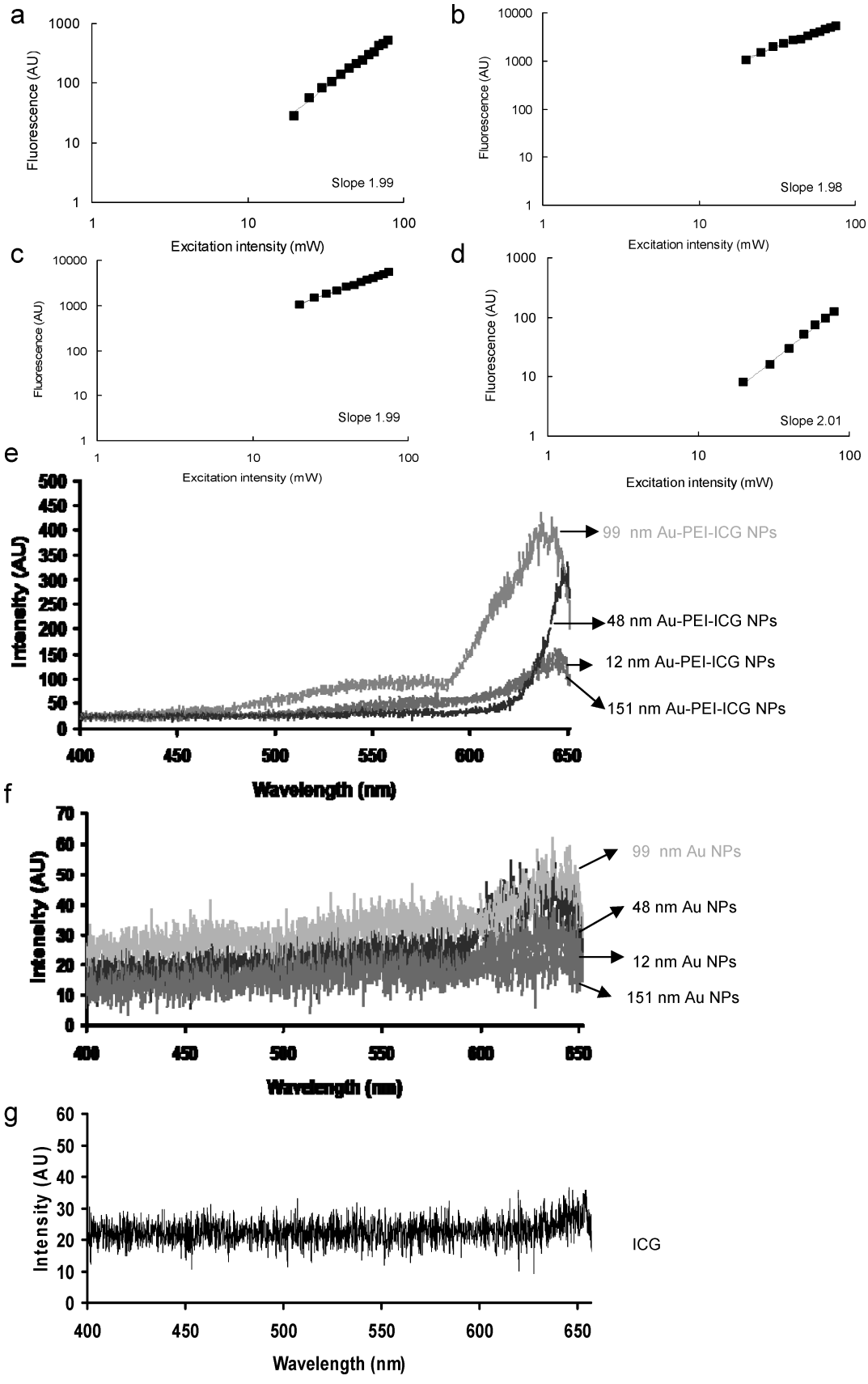

Figure 7. Dependence of two-photon excited fluorescence on excitation intensity[20] for (a) 12, (b) 48, (c) 99, and (d) 151 nm Au−PEI−ICG NPs, which were exposed to the femtosecond laser from 20 to 80 mW. The slope is shown in each figure. $R^2 > 0.99$. TPF spectrum of (e) 12, 48, 99, and 151 nm Au−PEI−ICG NPs; and (f) 12, 48, 99, and 151 nm Au NPs; and (g) ICG in order, which were exposed to the femtosecond laser at 5.0 mW.

DOI: 10.1021/acsami.5b04431
ACS Appl. Mater. Interfaces 2015, 7, 17318−17329

Table 2. Two-Photon Action Cross Sections of Au−PEI−ICG NPs

	Au−PEI−ICG NPs			
	12 nm	48 nm	99 nm	151 nm
action cross section, $\eta\ \sigma_2$ (GM, 10^{-50}cm^{4}s/photon)	0.012	0.019	0.03	0.021

[a]Excitation wavelength: 720 nm (12 nm Au−PEI−ICG NPs), 740 nm (48 nm Au−PEI−ICG NPs), 750 nm (99 nm Au−PEI−ICG NPs), and 760 nm (151 nm Au−PEI−ICG NPs).

emission: 820 nm) in the cytoplasm after observing the cells by using laser confocal microscopy; however, no fluorescence was exhibited by the cells without ICG treatment or laser exposure (Figure 6a). The nucleus of a cell exhibited a normal morphology due to the 90% viability of ICG−Ab_{EGFR}-treated A549 cells (Figure 6c; Supporting Information, Figure S7d). In addition, the fluorescence intensity in A549 cells treated with various sizes of Au−PEI−ICG−Ab_{EGFR} (Figure 6d−g) was stronger than that in the cells shown in Figure 6b. It showed the phenomenon of metal-enhanced fluorescence, in which the fluorescence-emitting ability and photostability of weakly fluorescent species are increased because of the proximity of free electron-rich metals, such as noble metals.[1,2,7] A549 cells were damaged by multiphoton laser exposure, and they underwent photodestruction, resulting in the nuclear cleavage of DNA (with the indication of yellow arrows) and formation of an apoptotic body (Figure 6h−k). Except for long-term stability[32] and EDX measurement (Supporting Information, Figures S8 and S9), the TPF spectra of the Au−PEI−ICG NPs were examined to further discuss the photostability to determine the potential of the contrast probe. In the past, the cross section of two-photon excitation, an essential parameter for multiphoton microscopy,[7] of many common fluorophores[20−22,33−35] and fluorescent proteins[36−38] were measured. In this work, the measurement was conducted. First of all, it is necessary to verify TPF from Au−PEI−ICG NPs by measuring the dependence of the fluorescence intensity on the excitation power.[23] Previous studies[2,16,39−41] have reported that the process of single-photon fluorescence (SPF) from noble metals.[2,14] Moreover, the mechanism involved in SPF-generated TPF, which was enhanced by several orders of magnitude, was similar to that involved in the generation of SPF by resonant coupling with localized surface plasmons produced by metals.[41−43] Figure 7a−d shows the dependence of fluorescence intensity[20] on the excitation power. The dependence was observed to be quadratic, with exponents of 1.98 to 2.01 measured for increasing excitation powers with a wavelength range of 720−820 nm, determining the excitation is a two-photon process.[29] Rhodamine B was selected as the standard reference for the action cross section.[20−22] After calculation, the results of action cross section of two-photon excitation for Au−PEI−ICG NPs were summarized in Table 2. Results show this photoparameter also increased depending on the diameter of the Au NPs within 100 nm. Figure 7e−g shows TPF spectra measured for the Au−PEI−ICG NPs, Au NPs of various sizes, and ICG with irradiation. Broad peaks around 580−650 nm are shown in Figure 7e, but the other broad peak was observed only at approximately 640−650 nm, likely because the marked thermal degradation mediated to accelerate the instability of ICG[2] through irradiation (Figure 7g). A higher intensity was observed in the spectrum of the Au−PEI−ICG NPs than in the spectrum of the Au NPs of any size and ICG (Figure 7). The interaction between the Au NPs and ICG caused oscillating dipoles; therefore, the two-photon photoproperties of ICG led to obvious enhancement.[2,44−46] Consequently, based on the examination of laser exposure, the Au NPs stabilized ICG, preventing the effect of thermal degradation, as well as processing and enhancing the metal enhanced fluorescence effect resulting from the high chemical stability and fluorescence intensities of the noble metals, and the photostability of the Au−PEI−ICG NPs.[2] These observations are consistent with those in Figure 6.[1] In addition, the photoproperty gradually increased depending on the diameter of the Au NPs within 100 nm.

An in-depth understanding of the excited-state process would facilitate efficient study of the surface modification of fluorophore−metallic NPs for photoproperties. Intermolecular interactions, fluorophore emission, and energy and electron transfer are the possible pathways of photoinduction that enhance the photoproperties of fluorophores bound on metallic NPs. The energy transfer process is considered the main pathway for the organic molecules conjugated on the surface of metallic NPs.[25] However, this essentially relies on the size and shape of NPs.[47] Owing to the resonant radiation, the oscillation of electrons to induce surface electric fields and the plasmon resonance considerably enhanced the properties of NPs.[2,7,15] Furthermore, because of the interaction between excited-state fluorophores and metallic nanomaterials, the free electrons in metals oscillate with fluorophores and exhibit dipole behavior,[2] resulting in clear enhancement of the absorption, emission, and stability of fluorophores and photochemical reactions. Consequently, these properties enable the Au−PEI−ICG NPs to exhibit higher photostability and photoefficiency in PDT and PTT. Therefore, as the size effect of the NPs with a diameter within 100 nm increased, they exhibited a more apparent effect after treatment with femtosecond laser irradiation. By contrast, the Au NPs with a diameter over 100 nm[48−50] were less photostable after coating their surfaces with ICG, and demonstrated lower photodestructive efficiency in killing bacteria and cancer cells compared with the NPs with a diameter within 100 nm.

CONCLUSION

Gold nanomaterials stabilize the ICG, preventing photodegradation from occurring, even through the exposure of nonlinear multiphoton laser. The Au−PEI−ICG NPs show remarkable photochemical destruction ability and contrast probe properties. Thus, Au−PEI−ICG NPs can be simultaneously used as more effective PDT and PTT agents. By using Au nanomaterials, the combined PDT and PTT killed MRSA and A549 cells more efficiently and improved photodestructive efficacy compared with ICG treatment alone. As a result, an additive effect was exerted in the therapeutic efficiency of the Au nanomaterials. The size-dependent effect of the Au NPs affected the photostability, photochemical effectiveness, two-photon fluorescence and two-photon excitation action cross section increased with an increase in the size of the NPs, but this was only observed in the NPs with a diameter within 100 nm. By contrast, compared with the NPs with a diameter within 100 nm, those with a diameter over 100 nm exhibited lower photostability and photodestructive efficiency in killing bacteria and A549 cells, as well as two-photon fluorescence and two-photon excitation action cross section. With the rapid increase in multidrug-resistant bacterial strains and malignant tumors, Au−PEI−ICG NPs are expected to be an alternative and

DOI: 10.1021/acsami.5b04431
ACS Appl. Mater. Interfaces 2015, 7, 17318−17329

potential therapeutic approach for ablating cancer cells and killing bacteria by irradiating them through nonlinear laser exposure.

■ ASSOCIATED CONTENT

Supporting Information

Two-photon fluorescence spectra and intensities, stability test, FTIR spectra, survival rates of bacteria, long-term cellular viabilities, EDX, two-photon action cross sections, and internalization of Au particle number. The Supporting Information is available free of charge on the ACS Publications website at DOI: 10.1021/acsami.5b04431.

■ AUTHOR INFORMATION

Corresponding Authors

*E-mail: wenshuokuo@mail.ncku.edu.tw.
*E-mail: a122@mail.ncku.edu.tw.

Present Address

▲National Cheng Kung University, No. 1, University Rd., Tainan 701, Taiwan.

Author Contributions

△These authors contributed equally to this work.

Notes

The authors declare no competing financial interest.

■ ACKNOWLEDGMENTS

This research was supported by the Ministry of Science and Technology, Taiwan (MOST-103-2113-M-006-010-MY2).

■ ABBREVIATIONS

Au = gold
NIR = near-infrared
PTT = photothermal therapy
ICG = indocyanine green
PDT = photodynamic therapy
ROS = reactive oxygen species
NP = nanoparticle
MRSA = methicillin-resistant *Staphylococcus aureus*
A549 = human lung carcinoma malignant cells
PEI = polyethylenimine
UV−vis = ultraviolet−visible spectroscopy
FTIR = Fourier transform infrared
EGFR = epidermal growth factor receptor
AA = atomic absorption
TPA = two-photon absorption
CFU = colony forming unit
TPF = two-photon fluorescence
SPF = single-photon fluorescence
TEM = transmission electron microscopy

■ REFERENCES

(1) Kuo, W. S.; Chang, C. N.; Chang, Y. T.; Yeh, C. S. Antimicrobial Gold Nanorods with Dual-Modality Photodynamic Inactivation and Hyperthermia. *Chem. Commun.* **2009**, 4835−4837.

(2) Kuo, W. S.; Chang, Y. T.; Cho, K. C.; Chiu, K. C.; Lien, C. H.; Yeh, C. S.; Chen, S. J. Gold Nanomaterials Conjugated with Indocyanine Green for Dual-Modality Photodynamic and Photothermal Therapy. *Biomaterials* **2012**, *33*, 3270−3278.

(3) Mirkin, C. A. Programming the Assembly of Two- and Three-Dimensional Architectures with DNA and Nanoscale Inorganic Building Blocks. *Inorg. Chem.* **2000**, *39*, 2258−2272.

(4) Orendorff, C. J.; Cole, A.; Sau, T. K.; Murphy, C. J. Surface-Enhanced Raman Spectroscopy of Self-Assembled Monolayers: Sandwich Architecture and Nanoparticle Shape Dependence. *Anal. Chem.* **2005**, *77*, 3261−3266.

(5) MacBeach, G.; Schreiber, S. Printing Proteins as Microarrays for High-Throughput Function Determination. *Science* **2000**, *289*, 1760−1763.

(6) Kuo, W. S.; Wu, C. M.; Yang, Z. S.; Chen, S. Y.; Chen, C. Y.; Huang, C. C.; Li, W. N.; Sun, C. K.; Yeh, C. S. Biocompatible Bacteria@Au Composites for Application in the Photothermal Destruction of Cancer Cells. *Chem. Commun.* **2008**, 4430−4432.

(7) Kuo, W. S.; Chang, C. N.; Chang, Y. T.; Yang, M. H.; Chien, Y. H.; Chen, S. J.; Yeh, C. S. Gold Nanorods in Photodynamic Therapy, as Hyperthermia Agents, and in Near-Infrared Optical Imaging. *Angew. Chem., Int. Ed.* **2010**, *49*, 2711−2715.

(8) Philip, P.; Penzkofer, A.; Bäumler, W.; Szeimies, R. M.; Abels, C. Absorption and Fluorescence Spectroscopic Investigation of Indocyanine Green. *J. Photochem. Photobiol., A* **1996**, *96*, 137−148.

(9) DeCoste, S. D.; Farinelli, W.; Flotte, T.; Anderson, R. R. Dye-Enhanced Laser Welding for Skin Closure. *Lasers Surg. Med.* **1992**, *12*, 25−32.

(10) Khlebtsov, B.; Zharov, V.; Melnikov, A.; Tuchin, V.; Khlebtsov, N. Optical Amplification of Photothermal Therapy with Gold Nanoparticles and Nanoclusters. *Nanotechnology* **2006**, *17*, 5167−5179.

(11) Geddes, C. D.; Parfenov, A.; Roll, D.; Uddin, J.; Lakowicz, J. R. Fluorescence Spectral Properties of Indocyanine Green on a Roughened Platinum Electrode: Metal-Enhanced Fluorescence. *J. Fluoresc.* **2003**, *13*, 453−457.

(12) Grabar, K. C.; Freeman, R. G.; Hommer, M. B.; Natan, M. L. Preparation and Characterization of Au Colloid Monolayers. *Anal. Chem.* **1995**, *67*, 735−743.

(13) Au, L.; Zhang, Q.; Cobley, C. M.; Gidding, M.; Schwartz, A. G.; Chen, J.; Xia, Y. Quantifying the Cellular Uptake of Antibody-Conjugated Au Nanocages by Two-Photon Microscopy and Inductively Coupled Plasma Mass Spectrometry. *ACS Nano* **2010**, *4*, 35−42.

(14) Kuo, W. S.; Lien, C. H.; Cho, K. C.; Chang, C. Y.; Lin, C. Y.; Huang, L.L. H.; Campagnola, P. J.; Dong, C. Y.; Chen, S. J. Multiphoton Fabrication of Freeform Polymer Microstructures with Gold Nanorods. *Opt. Express* **2010**, *18*, 27550−27559.

(15) Lien, C. H.; Kuo, W. S.; Cho, K. C.; Lin, C. Y.; Su, Y. D.; Huang, L. L.; Campagnola, P. J.; Dong, C. Y.; Chen, S. J. Fabrication of Gold Nanorods-Doped, Bovine Serum Albumin Microstructures via Multiphoton Excited Photochemistry. *Opt. Express* **2011**, *19*, 6260−6268.

(16) Wang, H.; Huff, T. B.; Zweifel, D. A.; He, W.; Low, P. S.; Wei, A.; Cheng, J. X. In Vitro and In Vivo Two-Photon Luminescence Imaging of Single Gold Nanorods. *Proc. Natl. Acad. Sci. U. S. A.* **2005**, *102*, 15752−15756.

(17) Zhou, G.; Gu, M. Direct Optical Fabriation of Three-Dimensional Photonic Crystals in a High Refractive Index $LiNbO_3$ Crystal. *Opt. Lett.* **2006**, *31*, 2783−2785.

(18) Joshi, A.; Punyani, S.; Bale, S. S.; Yang, H. C.; Borca-Tasciuc, T.; Kane, R. S. Nanotubes- Assisted Protein Deactivation. *Nat. Nanotechnol.* **2008**, *3*, 41−45.

(19) Misra, B. R.; Misra, H. P. Vasoactive Intestinal Peptide, a Singlet Oxygen Quencher. *J. Biol. Chem.* **1990**, *265*, 15371−15374.

(20) Xu, C.; Webb, W. W. Measurement of Two-Photon Excitation Cross Sections of Molecular Fluorophores with Data from 690 to 1050 nm. *J. Opt. Soc. Am. B* **1996**, *13*, 481−491.

(21) Cheng, L. C.; Horton, N. G.; Wang, K.; Chen, S. J.; Xu, C. Measurement of Multiphoton Action Cross Sections for Multiphoton Microscopy. *Biomed. Opt. Express* **2014**, *5*, 3427−3433.

(22) Xu, C.; Zipfel, W.; Shear, J. B.; Williams, R. M.; Webb, W. W. Multiphoton Fluorescence Excitation: New Spectral Windows for Biological Nonlinear Microscopy. *Proc. Natl. Acad. Sci. U. S. A.* **1996**, *93*, 10763−10786.

(23) Durr, N. J.; Larson, T.; Smith, D. K.; Korgel, B. A.; Sokolov, K.; Ben-Yakar, A. Two-Photon Luminescence Imaing of Cancer Cells Using Molecularly Targeted Gold Nanorods. *Nano Lett.* **2007**, *7*, 941−945.

DOI: 10.1021/acsami.5b04431
ACS Appl. Mater. Interfaces 2015, 7, 17318−17329

(24) Ren, F.; Bhana, S.; Norman, D. D.; Johnson, J.; Xu, J.; Baker, D. L.; Parrill, A. L.; Huang, X. Gold Nanorods Carrying Paclitaxel for Photothermal-Chemotherapy of Cancer. *Bioconjugate Chem.* **2013**, *24*, 376−386.
(25) Thomas, K. G.; Kamat, P. V. Chromophore-Functionalized Gold Nanoparticles. *Acc. Chem. Res.* **2003**, *36*, 888−898.
(26) Kamat, P. V. Photophysical, Photothermal and Photocatalytic Aspects of Metal Nanoparticles. *J. Phys. Chem. B* **2002**, *106*, 7729−7744.
(27) Fink, J.; Kiely, C.; Bethell, D.; Schiffrin, D. J. Self-Organization of Nanosized Gold Particles. *Chem. Mater.* **1998**, *10*, 922−926.
(28) Henglein, A.; Meisel, D. Spectrophotometric Observations of the Adsorption of Organosulfur Compounds on Colloidal Silver Nanoparticles. *J. Phys. Chem. B* **1998**, *102*, 8364−8366.
(29) Cho, K. C.; Lien, C. H.; Lin, C. Y.; Chang, C. Y.; Huang, L. L. H.; Campagnola, P. J.; Dong, C. Y.; Chen, S. J. Enhanced Two-Photon Excited Fluorescnece in Three-Dimensionally Crosslinked Bovine Serum Albumin Microstructures. *Opt. Express* **2011**, *19*, 11732−11739.
(30) Liu, S.; Zeng, T. H.; Hofmann, M.; Burcombe, E.; Wei, J.; Jiang, R.; Kong, J.; Chen, Y. Antibacterial Activity of Graphite, Graphite Oxide, Graphene Oxide and Reduced Graphene Oxide: Membrane and Oxidation Stree. *ACS Nano* **2011**, *5*, 6971−6980.
(31) Geddes, C. D.; Cao, H.; Gryczynski, I.; Gryczynski, Z.; Fang, J.; Lakowicz, J. R. Metal-Enhanced Fluorescence (MEF) Due to Silver Colloid on a Planar Surface: Potential Applications of Indocyanine Green to In Vivo Imaging. *J. Phys. Chem. A* **2003**, *103*, 3443−3449.
(32) Engel, E.; Schraml, R.; Maisch, K.; König, B.; Szeimies, R. M.; Hillenkamp, J.; Bäumler, W.; Vasold, R. Light-Induced Decomposition of Indocyanine Green. *Invest. Ophthalmol. Visual Sci.* **2008**, *49*, 1777−1783.
(33) Albota, M. A.; Xu, C.; Webb, W. W. Two-Photon Fluorescence Excitation Cross Sections of Biomolecular Probes from 690 to 960 nm. *Appl. Opt.* **1998**, *37*, 7352−7356.
(34) Makarov, S.; Drobizhev, M.; Rebane, A. Two-Photon Absorption Standards in the 550−1600 nm Excitation Wavelength Range. *Opt. Express* **2008**, *16*, 4029−4047.
(35) Mütze, J.; Iyer, V.; Macklin, J. J.; Colonell, J.; Karsh, B.; Petrášek, Z.; Schwille, P.; Looger, L. L.; Lavis, L. D.; Harris, T. D. Excitation Spectra and Brightness Optimization of Two-Photon Excited Probes. *Biophys. J.* **2012**, *102*, 934−944.
(36) Blab, G. A.; Lommerse, P. H. M.; Cognet, L.; Harms, G. S.; Schmidt, T. Two-Photon Excitation Action Cross-Sections of the Autofluorescent Proteins. *Chem. Phys. Lett.* **2001**, *350*, 71−77.
(37) Drobizhev, M.; Tillo, S.; Makarov, N. S.; Hughes, T. E.; Rebane, A. Absolute Two-Photon Absorption Spectra and Two-Photon Brightness of Orange and Red Fluorescent Proteins. *J. Phys. Chem. B* **2009**, *113*, 855−859.
(38) Drobizhev, M.; Makarov, N. S.; Tillo, S. E.; Hughes, T. E.; Rebane, A. Two-Photon Absorption Properties of Fluorescent Proteins. *Nat. Methods* **2011**, *8*, 393−399.
(39) Imura, K.; Nagahara, T.; Okamoto, H. Near-Field Two-Photon-Induced Photoluminescence from Single Gold Nanorods and Imaging of Plasmon Modes. *J. Phys. Chem. B* **2005**, *109*, 13214−13220.
(40) Mooradian, A. Photoluminescence of Metal. *Phys. Rev. Lett.* **1969**, *22*, 185−187.
(41) Boyd, G. T.; Yu, Z. H.; Shen, Y. R. Photoinduced Luminescence from the Noble Metals and its Enhancement on Roughened Surfaces. *Phys. Rev. B: Condens. Matter Mater. Phys.* **1986**, *33*, 7923−7936.
(42) Chen, C. K.; Castro, A. R. B. d.; Shen, Y. R. Surface-Enhanced Second-Harmonic Generation. *Phys. Rev. Lett.* **1981**, *46*, 145−148.
(43) Dickson, R. M.; Lyon, L. A. Unidirectional Plasmon Propagation in Metallic Nanowires. *J. Phys. Chem. B* **2000**, *104*, 6095−6098.
(44) Chance, R. R.; Prock, A.; Silbey, R. Molecular Fluorescence and Energy Transfer Near Interfaces. *J. Chem. Phys.* **1978**, *37*, 1−65.
(45) Gersten, J. I.; Nitzan. Accelerated Energy Tansfer Between Molecules Near a Solid Particle. *Chem. Phys. Lett.* **1984**, *104*, 31−37.
(46) Gersten, J. I.; Nitzan, A. Spectroscopic Properties of Molecules Interacting with Small Dielectric Particles. *J. Chem. Phys.* **1981**, *75*, 1139−1152.
(47) Thomas, K. G.; Kamat, P. V. Chromophore-Functionalized Gold Nanoparticles. *Acc. Chem. Res.* **2003**, *36*, 888−898.
(48) Frens, G. Controlled Nucleation for the Regulation of the Particle Size in Monodisperse Gold Suspensions. *Nature, Phys. Sci.* **1973**, *241*, 20−22.
(49) Link, S.; El-Sayed, M. A. Shape and Size Dependence of Radiative, Non-Radiative and Photothermal Properties of Gold Nanocrystals. *Int. Rev. Phys. Chem.* **2000**, *19*, 409−453.
(50) Jiang, W.; Kim, B. Y.; Rutka, J. T.; Chan, W. C. W. Nanoparticle Mediated Cellular Response is Size-Dependent. *Nat. Nanotechnol.* **2008**, *3*, 145−150.

DOI: 10.1021/acsami.5b04431
ACS Appl. Mater. Interfaces 2015, 7, 17318−17329